




Low Levels of T Cell Exhaustion in Tuberculous Lung Granulomas

Eileen A. Wong,^a Louis Joslyn,^b Nicole L. Grant,^c Edwin Klein,^d Philana Ling Lin,^e Denise E. Kirschner,^b  JoAnne L. Flynn^a

^aDepartment of Microbiology and Molecular Genetics, University of Pittsburgh School of Medicine, Pittsburgh, Pennsylvania, USA

^bDepartment of Microbiology and Immunology, University of Michigan Medical School, Ann Arbor, Michigan, USA

^cDepartment of Infectious Disease and Microbiology, University of Pittsburgh Graduate School of Public Health, Pittsburgh, Pennsylvania, USA

^dDivision of Laboratory Animal Research, University of Pittsburgh, Pittsburgh, Pennsylvania, USA

^eDepartment of Pediatrics, University of Pittsburgh School of Medicine and Children's Hospital of UPMC, Pittsburgh, Pennsylvania, USA

ABSTRACT The hallmarks of pulmonary *Mycobacterium tuberculosis* infection are lung granulomas. These organized structures are composed of host immune cells whose purpose is to contain or clear infection, creating a complex hub of immune and bacterial cell activity, as well as limiting pathology in the lungs. Yet, given cellular activity and the potential for frequent interactions between host immune cells and *M. tuberculosis*-infected cells, we observed a surprisingly low quantity of cytokine-producing T cells (<10% of granuloma T cells) in our recent study of *M. tuberculosis* infection within nonhuman primate (NHP) granulomas. Various mechanisms could limit T cell function, and one hypothesis is T cell exhaustion. T cell exhaustion is proposed to result from continual antigen stimulation, inducing them to enter a state characterized by low cytokine production, low proliferation, and expression of a series of inhibitory receptors, the most common being PD-1, LAG-3, and CTLA-4. In this work, we characterized the expression of inhibitory receptors on T cells and the functionality of these cells in tuberculosis (TB) lung granulomas. We then used these experimental data to calibrate and inform an agent-based computational model that captures environmental, cellular, and bacterial dynamics within granulomas in lungs during *M. tuberculosis* infection. Together, the results of the modeling and the experimental work suggest that T cell exhaustion alone is not responsible for the low quantity of *M. tuberculosis*-responsive T cells observed within TB granulomas and that the lack of exhaustion is likely an intrinsic property of granuloma structure.

KEYWORDS *Mycobacterium tuberculosis*, T cell exhaustion, computational biology, granuloma

Tuberculosis (TB), caused by inhalation of the bacterium *Mycobacterium tuberculosis*, continues to be a major global health problem. The World Health Organization estimates that more than 10 million people became ill with TB in 2016 alone and that 1.7 million deaths were caused by TB (1). TB is a chronic pulmonary disease, with organized structures, called granulomas, forming within the lungs and thoracic lymph nodes. Granulomas are formed by the host immune response to *M. tuberculosis*. Due to the substantial heterogeneity of granulomas, even within the same host, these structures can contain and kill *M. tuberculosis* but also can be a niche for bacterial survival, replication, and persistence (2). The host immune cells and *M. tuberculosis* bacilli and antigens interact within the granulomas for the entire course of infection, which, during

Received 30 May 2018 Accepted 1 June 2018

Accepted manuscript posted online 11 June 2018

Citation Wong EA, Joslyn L, Grant NL, Klein E, Lin PL, Kirschner DE, Flynn JL. 2018. Low levels of T cell exhaustion in tuberculous lung granulomas. *Infect Immun* 86:e00426-18. <https://doi.org/10.1128/IAI.00426-18>.

Editor Andreas J. Bäumer, University of California, Davis

Copyright © 2018 American Society for Microbiology. All Rights Reserved.

Address correspondence to Denise E. Kirschner, kirschne@umich.edu, or JoAnne L. Flynn, joanne@pitt.edu.

E.A.W. and L.J. contributed equally to this work.

clinically latent TB, can last the lifetime of the host (3). Macrophages are the primary host cell for infection, while CD4⁺ and CD8⁺ T cells have been shown to be critical for granuloma formation and maintenance through cytokine secretion and activation of other immune cells, including macrophages (4, 5). Yet, even though the granuloma provides the potential for frequent interactions between host immune cells and *M. tuberculosis* bacilli, our previous data in a macaque model showed that less than 10% of T cells in a granuloma produce cytokines (6). While various mechanisms could be limiting T cell function, one potential explanation for the low T cell responses within granulomas is T cell exhaustion occurring due to chronic antigen stimulation from *M. tuberculosis*-infected cells.

In chronic viral infections and cancer, a subpopulation of T cells has been demonstrated to lose both functionality and proliferation capabilities over time in response to persistent antigen stimulation (7–12). This subpopulation of T cells enters an “exhausted” state, characterized by low cytokine production, low proliferation, and expression of a series of inhibitory receptors. The most well studied of these receptors include PD-1, CTLA-4, and LAG-3, which interact with a range of ligands to activate negative regulatory pathways (13, 14). While these inhibitory receptors may balance an overly activated immune response that could lead to disease pathology, the receptors can also prevent an effective immune response from clearing infections and tumor cells. In cancer and some infectious diseases, a blockade of these inhibitory receptors reverses exhaustion and rescues T cell functions (15–19).

Since *M. tuberculosis* causes a chronic bacterial infection confined to a structured environment, it seems obvious that T cell exhaustion would occur within the critical site of granulomas. Not surprisingly, the contribution of T cell exhaustion to TB has been the subject of several studies. Patients with active TB have been shown to have significantly higher PD-1 expression on their peripheral blood mononuclear cells (PBMC) than healthy controls, and blockade of inhibitory receptors *in vitro* enhanced T cell function (20–22). Additionally, increased antigen load was associated with decreased T cell responses in patients with high *M. tuberculosis* loads compared to patients with latent *M. tuberculosis* infections (23). Rhesus macaques with active or reactivated TB expressed more LAG-3 on their CD3⁺ T cells in their lung tissue than clinically latent animals (24). PD-1 expression significantly correlated with CTLA-4 expression on CD4⁺ T cells from tissues of *M. tuberculosis*-infected rhesus macaques (25). *M. tuberculosis* infections in mice increased the expression of PD-1 and LAG-3 as the infection progressed, and this was associated with increased T cell impairment (26). However, murine studies also suggested that the presence of these inhibitory receptors may be beneficial for overall TB disease pathology and bacterial control and are necessary to maintain antigen-specific effector T cells during *M. tuberculosis* infections (27, 28), with detrimental outcomes when mice lacking PD-1 were infected with *M. tuberculosis* (29–31). While these studies examined T cell exhaustion in the periphery (patient studies) or in the whole lung (animal models), the frequency and role of exhausted T cells in individual granulomas are still unstudied and could provide important clues to overall infection dynamics, as granulomas are the sites of infection in pulmonary TB. Confounding these data, the relationship between inhibitory markers and functional exhaustion is not abundantly clear. Recent studies have shown that inhibitory receptors can act as activation markers and that T cells can simultaneously express both inhibitory and activation markers (14, 32–35). Therefore, it becomes difficult to distinguish T cell exhaustion using inhibitory receptors alone.

We hypothesized that T cell exhaustion could be contributing to the observed low frequencies of T cells producing cytokines in TB granulomas. We used a nonhuman primate (NHP) model of TB that recapitulates human granuloma structure and disease to assess the extent of exhausted T cells and their function in lung granulomas (36). However, contrary to our hypothesis, we found low levels of inhibitory receptor expression, and those T cells expressing inhibitory receptors were often still functional. To further confirm and explore these findings, we applied a computational modeling approach using GranSim, our agent-based model simulator of lung granulomas. The

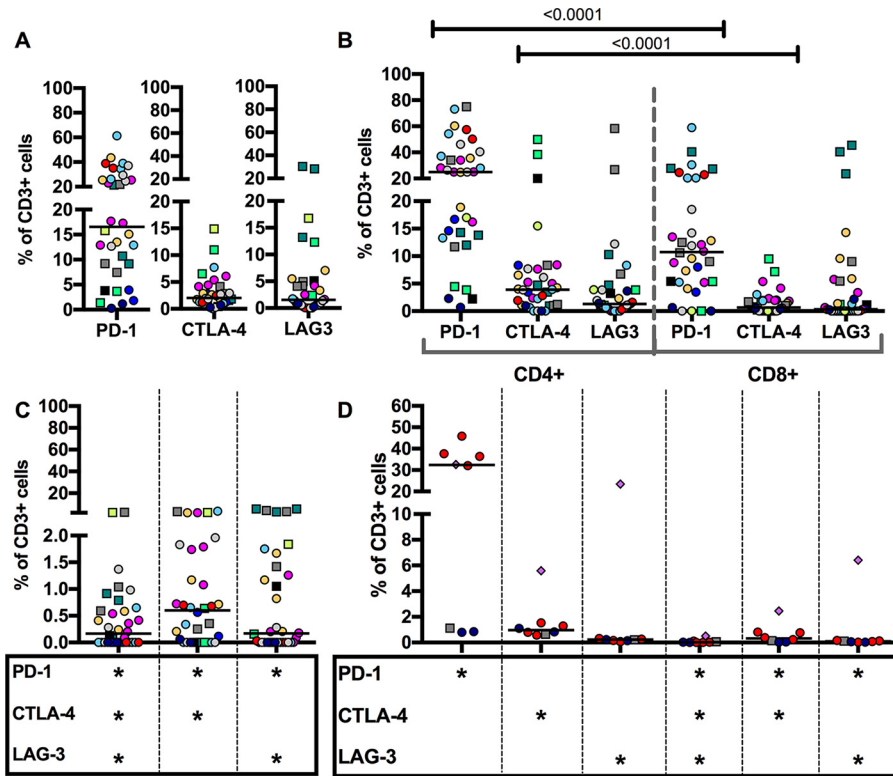


FIG 1 Few T cells in granulomas of *M. tuberculosis*-infected macaques coexpress inhibitory receptors. (A) Frequency of CD3⁺ cells expressing inhibitory receptors PD-1, CTLA-4, or LAG-3 in individual granulomas from *M. tuberculosis*-infected cynomolgus or rhesus macaques. (B) CD4 T cells express inhibitory receptors more frequently than CD8 T cells. *P* values indicated on the figure were determined by a Wilcoxon matched-pairs signed-rank test. (C) Frequency of coexpression of inhibitory receptors in granulomas. Each point indicates a granuloma, each color corresponds to an NHP (12 NHPs), circles indicate cynomolgus macaques, and squares indicate rhesus macaques. (D) Clusters of granulomas and TB pneumonia samples have similarly low frequencies of CTLA-4 and LAG3 and similarly high frequencies of PD-1 alone. There is low coexpression of inhibitory receptors in clusters of granulomas. Each point indicates a cluster, consolidation, or pneumonia lung sample, each color corresponds to an NHP (6 NHPs), circles indicate cynomolgus macaques, squares indicate rhesus macaques, and the diamond indicates a TB pneumonia sample. Horizontal lines indicate medians.

model predicts that the structure of granulomas may prevent T cell exhaustion, and we conclude that this mechanism is likely beneficial for the host because granulomas can remain functional even after chronic containment of *M. tuberculosis* from months to years. Thus, our data indicate that T cell exhaustion is limited in most tuberculous granulomas.

RESULTS

Few T cells in granulomas of *M. tuberculosis*-infected macaques coexpress inhibitory receptors. T cells from individual lung granulomas from *M. tuberculosis*-infected macaques (6 to 31 weeks postinfection) were characterized for expression of well-documented markers for T cell exhaustion, namely, the inhibitory receptors PD-1, CTLA-4, and LAG-3, using flow cytometry (Fig. 1A; see Table S1A in the supplemental material). PD-1 was expressed in higher frequencies (median, 16.55% of the CD3⁺ T cells), while the majority of the CD3⁺ T cells expressed very low frequencies of CTLA-4 (median, 2.02%) or LAG-3 (median, 1.53%) in granulomas. Although exhaustion in CD8 T cells has been more commonly characterized, exhausted CD4 T cells also comprise a critical and distinct population of exhausted T cells (37). In TB granulomas, the inhibitory receptors PD-1 and CTLA-4 tended to be expressed more frequently on CD4 T cells than on CD8 T cells (Fig. 1B). Thoracic lymph nodes infected with *M. tuberculosis* also had low levels of inhibitory receptor expression, including PD-1, relative to total CD3 populations (Fig. S3A).

Since these inhibitory receptors also have been characterized as markers of activation on T cells, coexpression of these inhibitory receptors has been demonstrated to be a better indicator of exhaustion (38). By flow cytometry, coexpression of inhibitory receptors on CD3⁺ T cells in any combination was rare (Fig. 1C; Table S1B). There were very few CD3⁺ T cells that had coexpression of these inhibitory receptors, with median levels of <2% of CD3⁺ T cells. In cynomolgus macaques, PD-1 and CTLA-4 had the highest levels of coexpression in granulomas, but this was still very low (median, 0.70%; interquartile range, 1.72%). In rhesus macaques, PD-1 and LAG-3 had the highest levels of coexpression, with a median of 2.98% of CD3⁺ T cells. Even in more severe forms of disease pathology (i.e., clusters of granulomas and consolidations, where the bacterial burden is often higher), expression of inhibitory receptors, including coexpression, was low, similar to that of individual granulomas (Fig. 1D; Table S1B). Notably, however, the sample of TB pneumonia, the most severe form of disease, had the highest expression of LAG-3, and 6.4% of the T cells from the sample coexpressed PD-1 and LAG-3 (Fig. 1D, diamonds).

Inhibitory receptors tend to be expressed on other immune cells in the granuloma. To further characterize T cell exhaustion in TB granulomas, we used immunohistochemistry to identify the spatial location of the few T cells coexpressing inhibitory receptors (Fig. 2). Granulomas from early in infection (6 weeks of *M. tuberculosis* infection) had an infiltration of T cells throughout the granuloma, with concentrated clusters of T cells in the outer periphery of the granuloma and limited but present caseous necrosis. Cell populations in immunohistochemistry images were quantified using CellProfiler. LAG-3⁺ CD3⁺ cells (4.348% of CD3⁺ cells) were identified close to the periphery of the granuloma, but the majority of LAG-3⁺ cells were not CD3⁺. Similarly, there were few PD-1⁺ CD3⁺ T cells identified in this particular section of granuloma (approximately 1.0%) (Fig. 2A to J). In contrast, granulomas from later in infection (≥ 12 weeks of *M. tuberculosis* infection) were more organized structures, with a region of necrosis in the middle (caseum) and fewer T cells spread throughout the granuloma, being mostly concentrated in the lymphocyte cuff away from the region of caseum. Despite differences in organization compared to that of early granulomas, later granulomas also had very few LAG-3⁺ CD3⁺ cells (1.191% of CD3⁺ cells) but a higher frequency of PD-1⁺ CD3⁺ cells than at 6 weeks (4.94% of CD3⁺ cells). The few PD-1⁺ CD3⁺ or LAG-3⁺ CD3⁺ cells were localized in the periphery of the granuloma (Fig. 2K to T).

In granulomas from both early and late stages in infection, most of the T cells in the granuloma had very little coexpression of CD3 with PD-1 or LAG-3, supporting our results observed by flow cytometry. Instead, most of the expression of these inhibitory receptors tended to be on other immune cells in the granuloma. While PD-1 colocalized with some of the CD3⁺ cells in the granuloma, LAG-3 was more often expressed on cells in the granuloma other than T cells. For example, in the samples at 6 and 20 weeks postinfection, 82.9% and 78.2% of the LAG-3⁺ cells were CD3⁻, respectively. While we were unable to confirm the identity of the LAG-3⁺ cells, other immune cell types can express LAG-3, including NK cells, B cells, macrophages, and plasmacytoid dendritic cells (39–42). Of the CD3⁺ cells expressing an inhibitory receptor, these cells tended to be in the periphery of the granuloma, further away from the necrotic center of the granuloma, where the *M. tuberculosis* bacilli are located.

T cells expressing inhibitory receptors are not functionally exhausted. Although few T cells in TB granulomas expressed inhibitory receptors, we investigated whether these rare cells were functionally exhausted. Exhausted T cells are characterized by hierarchical defects in function, beginning with decreased proliferation and interleukin-2 (IL-2) production, followed by decreased tumor necrosis factor (TNF) production, and finally decreased gamma interferon (IFN- γ) production (43). We examined the cytokine production by T cells expressing inhibitory receptors and found that some of these cells continued to express Ki67 (proliferation marker) and produce IL-2, TNF, and IFN- γ (Fig. 3). Overall, the functionality of T cells expressing so-called inhibi-

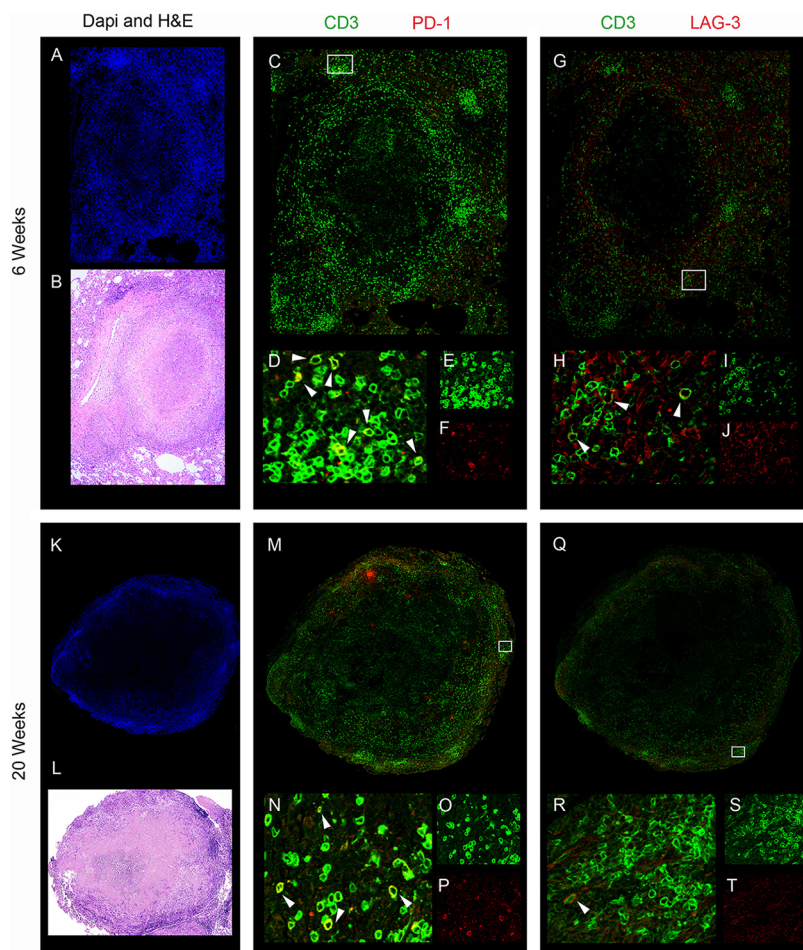


FIG 2 Example of spatial organization of inhibitory receptors on T cells within TB granulomas. Few T cells in lung granulomas express PD-1 or LAG-3 inhibitory receptors, and most of the expression of these inhibitory receptors are on other CD3⁻ cells. The rare CD3⁺ and PD-1⁺ or LAG-3⁺ coexpressing cells are localized in the periphery of the granuloma, away from the necrotic caseous center. Granulomas isolated at 6 weeks (A to J) and 20 weeks (K to T) were stained using antibodies against CD3, PD-1, and LAG-3 (see Materials and Methods for details). (A and K) DAPI staining of nuclei; (B and L) hematoxylin and eosin (H&E) staining; (C and M) merged image of CD3 (green) and PD-1 (red); (D and N) magnified region of interest (ROI) as indicated by a white box in panel C or M, where arrowheads indicate PD-1⁺ CD3⁺ cells; (E and O) magnified ROI showing green channel only (CD3); (F and P) magnified ROI showing red channel only (PD-1); (G and Q) merged image of CD3 (green) and LAG-3 (red); (H and R) magnified ROI, as indicated by a white box in panel G or Q, where arrowheads indicate LAG-3⁺ CD3⁺ cells; (I and S) magnified ROI showing green channel only (CD3); (J and T) magnified ROI of red channel only (LAG-3).

tory receptors were generally similar to that of the T cells not expressing inhibitory receptors.

While only about 3% of CD3⁺ T cells expressing PD-1 produced at least one of the cytokines usually lost in exhausted T cells, namely, IL-2, TNF, and IFN- γ (Th1; Fig. 3A), production was comparable to the cytokine response of CD3⁺ T cells not expressing PD-1 (median, 2.12%). Compared to CD3⁺ PD-1⁻ cells, significantly more CD3⁺ PD-1⁺ cells were expressing Ki67 (median, 2.54% CD3⁺ PD-1⁺ versus 0.04% CD3⁺ PD-1⁻ cells) or IFN- γ (median, 1.43% CD3⁺ PD-1⁺ versus 1.03% CD3⁺ PD-1⁻ cells), indicating ongoing and perhaps increased proliferation and functionality in cells expressing PD-1 (Fig. 3A). CD3⁺ CTLA-4⁺ cells and CD3⁺ LAG-3⁺ cells had a wide range of cytokine responses but still expressed Ki67 or cytokines at frequencies comparable to those of CD3⁺ cells negative for inhibitory receptors (Fig. 3B and C). The median Ki67 expression and cytokine response were low for CD3⁺ CTLA-4⁺ cells, but some cells produced cytokines at high frequencies, causing more spread in the interquartile ranges (IFN- γ , 0 to 10.02%; TNF, 0 to 7.678%; and Th1 cytokine, 0 to 17.1%) (Fig. 3B). About 1/10 of

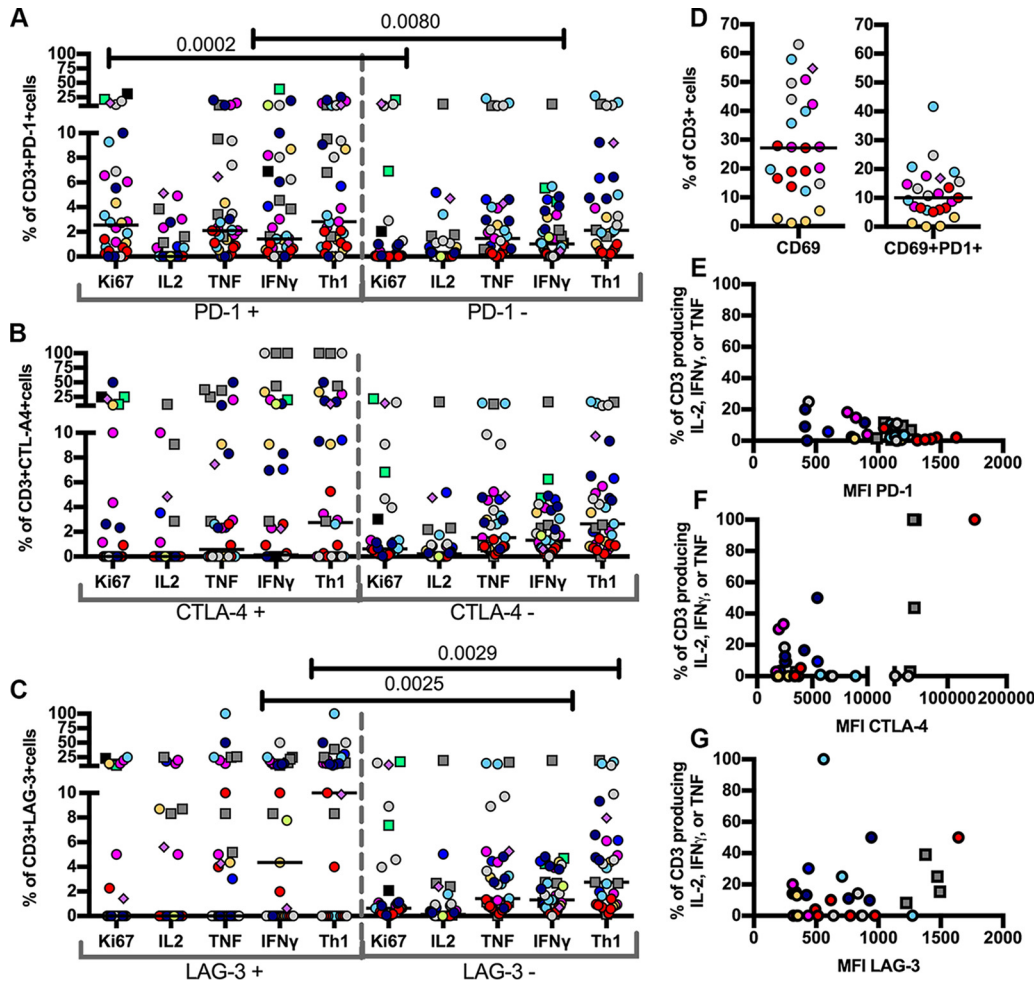


FIG 3 T cells from two species of NHP expressing inhibitory receptors in lung granulomas, granuloma clusters, and TB pneumonia samples remain functional. Cytokine and Ki67 (proliferation) expression from two NHP species were compared between CD3⁺ PD-1⁺ cells and CD3⁺ PD-1⁻ cells (*P* values: Ki67 = 0.0002, IL-2 = 0.7631, TNF = 0.1488, IFN- γ = 0.0080, Th1 = 0.0871) (A), CD3⁺ CTLA-4⁺ cells and CD3⁺ CTLA-4⁻ cells (*P* values: Ki67 = 0.8314, IL-2 = 0.4908, TNF = 0.5207, IFN- γ = 0.0542, Th1 = 0.0907) (B), CD3⁺ LAG3⁺ cells and CD3⁺ LAG3⁻ cells (*P* values: Ki67 = 0.6295, IL-2 = 0.3294, TNF = 0.2023, IFN- γ = 0.0025, Th1 = 0.0029) (C). Th1 refers to T cells producing IL-2, TNF, or IFN- γ . Each point indicates a lung sample (granuloma, granuloma cluster, or pneumonia), each color corresponds to an NHP (12 NHPs), circles indicate cynomolgus macaques, squares indicate rhesus macaques, and the diamond indicates a TB pneumonia sample. *P* values are from a Wilcoxon matched-pairs signed-rank test. (D) Frequency of CD69 expression on T cells in the granuloma and coexpression with PD-1 on T cells in the granuloma. Each point indicates a lung sample (granuloma or granuloma cluster), each color corresponds to an NHP (6 NHPs), and the diamond indicates a TB pneumonia sample. Horizontal lines indicate the medians. (E) Median fluorescence intensity (MFI) of expression of PD-1 (Spearman ρ = -0.4319, *P* = 0.0107) on CD3 T cells negatively correlates with cytokine production. (F and G) In contrast, MFI of CTLA-4 (Spearman ρ = 0.1612, *P* = 0.37) (F) and LAG-3 (Spearman ρ = 0.1343, *P* = 0.4712) (G) on CD3 T cells does not correlate with cytokine production. Each point indicates a lung sample (granuloma, granuloma cluster, or pneumonia), each color corresponds to an NHP (12 NHPs), circles indicate cynomolgus macaques, squares indicate rhesus macaques. Correlations were determined by the Spearman ρ test.

LAG-3-expressing CD3⁺ T cells still produced at least one of the cytokines, particularly IFN- γ , but the cells seemed to be split between cells not producing any cytokines or proliferation marker and those that continue to function (Fig. 3C). LAG-3⁺ CD3⁺ T cells had significantly higher frequencies of IFN- γ response, which likely also drove the significantly higher frequencies of LAG-3⁺ CD3⁺ T cells than of LAG-3⁻ CD3⁺ T cells expressing any of the Th1 proinflammatory cytokines (Fig. 3C). The T cells expressing inhibitory receptors in the most severe form of TB disease pathology, TB pneumonia, still show signs of proliferation and cytokine production (Fig. 3A, B, and C, diamonds). Generally, CD3⁺ T cells that also expressed an inhibitory receptor had similar or even

TABLE 1 Expression of inhibitory receptors on T cells in TB granulomas and complex TB disease is not correlated with bacterial burden^a

Comparison	Spearman ρ	Probability > $ \rho $
log CFU vs % PD-1	-0.0878	0.5804
log CFU vs % CTLA4	-0.1921	0.223
log CFU vs % LAG3	-0.212	0.1777
log CFU vs % PD-1 ⁺ CTLA-4 ⁺	-0.03	0.8506
log CFU vs % PD-1 ⁺ LAG-3 ⁺	0.0752	0.6358

^aFrequencies of CD3⁺ T cells expressing or coexpressing inhibitory receptors from TB granulomas and clusters do not correlate with their bacterial burdens, as measured by CFU.

higher frequencies of cytokine production or proliferation than CD3⁺ T cells without inhibitory receptors.

As many of the cells with inhibitory receptors still proliferate or produce cytokines, they are unlikely to be exhausted. In fact, it may be that these markers, at least when expressed singly, are actually identifying activated T cells within granulomas. Coexpression of PD-1 and CD69 on 10% of the T cells in the granulomas suggests that at least a portion of the few cells expressing inhibitory receptors in the granulomas are activated and not exhausted (Fig. 3D). Likewise, low cytokine response and proliferation activity of CD3⁺ T cells in *M. tuberculosis*-infected lymph nodes expressing inhibitory receptors likely result from the abundance of naive T cells, rather than T cell exhaustion present in the lymph nodes (Fig. S3). The intensity of PD-1 expression, as measured by median fluorescence intensity (MFI), on the T cells of the granulomas did negatively correlate with production of cytokines, suggesting that granulomas with higher expression of PD-1 may be more exhausted, although the correlation was modest (Spearman $\rho = -0.43$, $P = 0.01$) (Fig. 3E). There was no correlation between the intensity of CTLA-4 or LAG-3 expression and cytokine production, indicating that higher expression of CTLA-4 or LAG-3 on T cells does not correlate with less cytokine production (Fig. 3F and G). Blocking *M. tuberculosis*-infected samples *ex vivo* with anti-PD-1 and PD-L1 antibodies did not lead to markedly increased cytokine response or proliferation (Fig. S4), further supporting that PD-1 expression on T cells in *M. tuberculosis* does not necessarily indicate exhaustion. Together with the continued functionality of these cells (proliferation and cytokine production), these data suggest that the vast majority of T cells in the granuloma are not exhausted.

Expression of inhibitory receptors on T cells in TB granulomas is not correlated with bacterial burden. To determine whether the presence of potentially exhausted T cells in the TB granulomas was related to a higher bacterial burden or an inability to control infection, we tested the correlation of inhibitory receptor expression to the number of CFU of each individual granuloma. There was no correlation between frequency of CD3⁺ PD-1⁺, CD3⁺ CTLA-4⁺, or CD3⁺ LAG-3⁺ cells with the bacterial burden of each granuloma (Table 1). Frequencies of T cells coexpressing PD-1 and CTLA-4 or PD-1 and LAG-3 also did not correlate with the bacterial burden of the granuloma (Table 1).

Computational modeling reveals that granuloma structure may prevent T cell exhaustion. Our *in vivo* data do not support widespread T cell exhaustion within TB granulomas. Further, *in vivo* data could not answer the following questions about T cell exhaustion. (i) What are the temporal dynamics of exhaustion in the granuloma? (ii) Within the granuloma, are there areas where a T cell has a greater likelihood of becoming exhausted? (iii) Can we generally explain the presence of only low quantities of exhausted T cells? These questions require a technique that addresses both the spatial and temporal dynamics that are intrinsic to the development of a T cell exhaustion phenotype. To further explore the relationship between T cell exhaustion and granuloma function, we turned to our existing computational model, GranSim (44–49). We simulated a wide range of granuloma outcomes, creating a library of granulomas using the uncertainty analysis technique of Latin hypercube sampling (LHS) (50). We also incorporated various levels of exhausted T cell phenotypes to

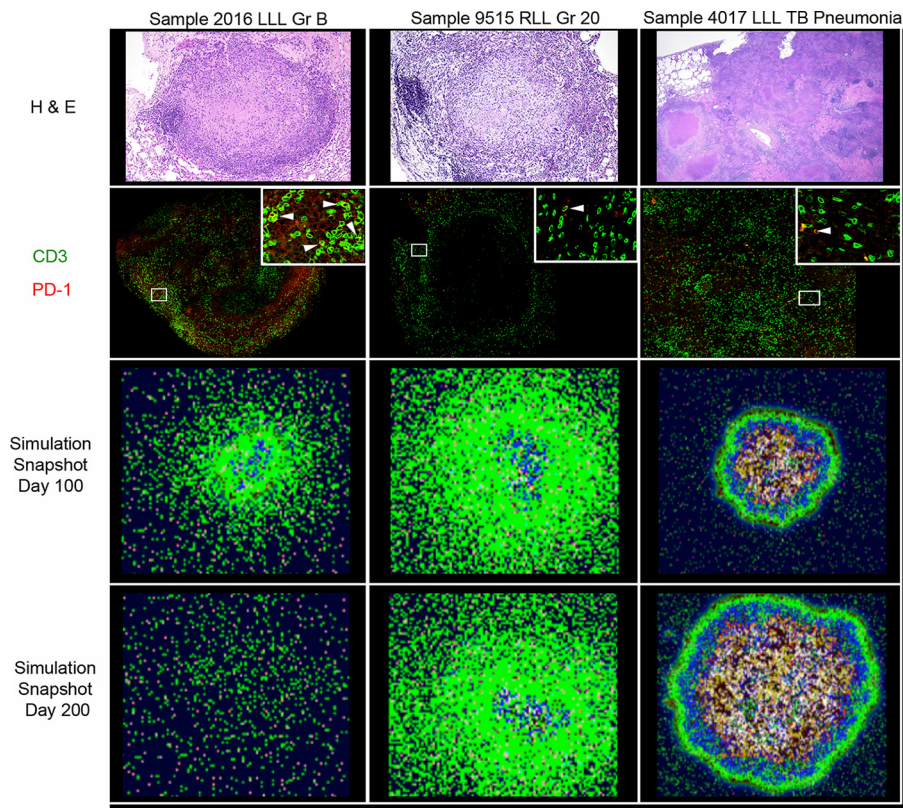


FIG 4 Comparison of macaque and simulated granulomas with various levels of bacterial burden. Row 1, H&E sections from granulomas excised from NHPs. Row 2, Immunohistochemistry (IHC) staining showing spatial organization of PD-1- and CD3-expressing cells in lung granulomas excised from NHPs (green = CD3, red = PD1). The inset is a magnification of the ROI (indicated by a white box), where arrowheads indicate PD-1⁺ CD3⁺ cells. Row 3, Simulated granuloma snapshots at day 100 (near the matching time of necropsy). Row 4, A snapshot prediction of the granuloma outcome if each simulation is continued until day 200. In both rows 3 and 4, colors indicate the following: green, resting macrophages; blue, activated macrophages; orange, infected macrophages; red, chronically infected macrophages; brown, extracellular bacteria; pink, gamma-producing T cells; purple, cytotoxic T cells; aqua, regulatory T cells; and white cross-hatched, caseated.

ascertain the effects of T cell exhaustion on granuloma outcomes. Finally, we evaluated T cell dynamics across infection time and space in order to develop a hypothesis to explain the low levels of exhaustion observed in the NHP studies herein.

After creating an *in silico* biorepository of 4,500 granulomas (see Materials and Methods), we found that every macaque granuloma sample has at least one corresponding simulation match. We selected three individual granuloma simulations that best matched the bacterial burden and CD3⁺ T cell counts of the three NHP granuloma samples, 2016_LLL GR B, 9515_RLL GR 20, 4017_LLL TB pneumonia, to investigate the potential roles of exhaustion in granulomas. These were chosen to represent a spectrum of granuloma outcomes: sterile, median bacterial load, and high bacterial load samples, respectively. We directly compared these three NHP samples and their corresponding simulations from GranSim (Fig. 4). In Fig. 4, the leftmost column represents a sample that was sterile at the time of necropsy (112 days postinfection, with 0 CFU), the middle column shows a sample with a median bacterial burden during the time of necropsy (84 days postinfection, with 600 CFU), and the far-right column displays a high-burden sample (70 days postinfection, with 138,000 CFU). The first row displays the hematoxylin and eosin (H&E) staining of sections, while the second row displays the PD-1 and CD3 expression in the matched granulomas. The third row displays an *in silico* snapshot taken at day 100 for each corresponding granuloma simulation (near the time of necropsy of the NHPs). The fourth row represents a prediction: each figure is an *in*

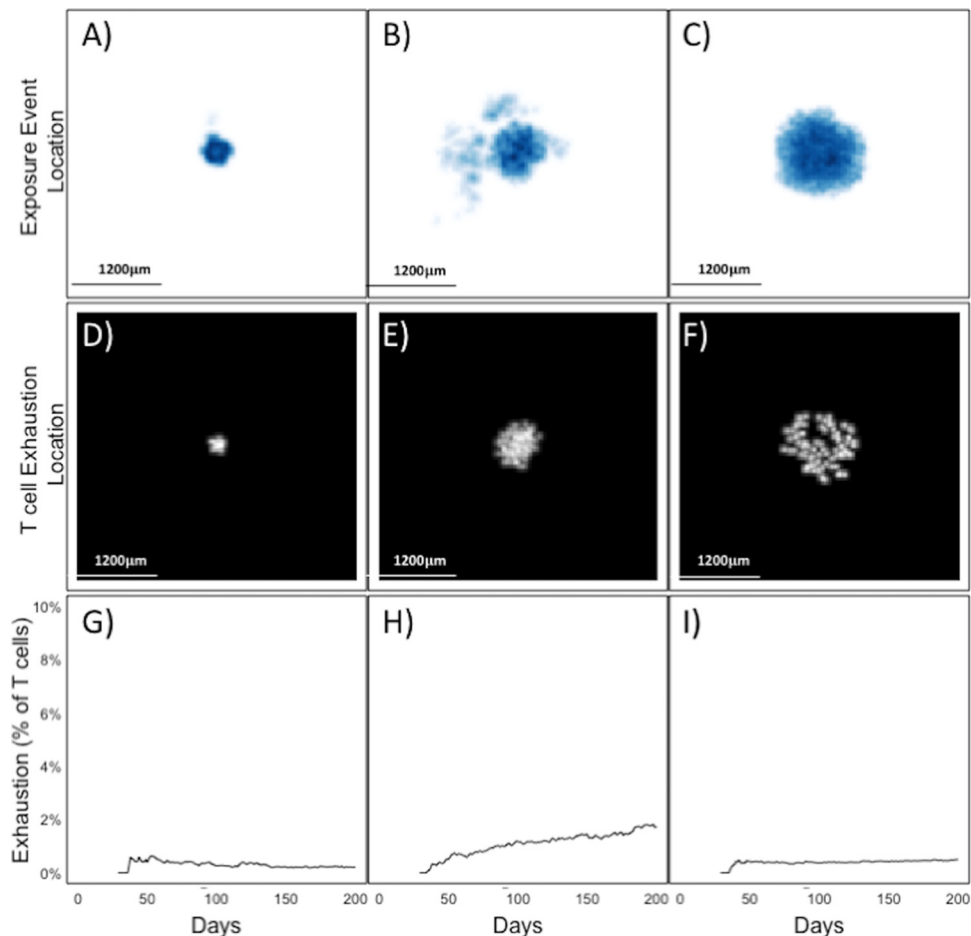


FIG 5 T cell location within granulomas prevents T cell exhaustion by reducing exposure events. (A, B, and C) Cloud maps showing the location of every EE in sterile, medium CFU, and TB pneumonia simulations. Dark blue represents areas of high numbers of EE, and white represents a lack of EE. (D, E, and F) Heat map location where T cells (cytotoxic or IFN- γ producers) became exhausted. White represents the location of T cells at the time of exhaustion. (G, H, and I) Time series graphs that display cumulative levels of exhaustion (as a percentage of total cytotoxic and IFN- γ producers) within simulations corresponding to panels A to C and panels D to F.

silico snapshot of the granuloma simulation at day 200. These comparisons support that the simulated granulomas both temporally and spatially capture the characteristics of the macaque granulomas.

Under the assumption that T cell exhaustion occurs upon repeated exposure to antigen, we defined an exposure event (EE) as the interaction between a T cell and an antigen-exposed macrophage in the granuloma. The range of EE across the 2,945 simulations that matched the 44 macaque granuloma samples was 205 to 9,199, with a median of 5,236. Therefore, a threshold of 5,236 EEs was set as a conservative estimate of our exhaustion threshold, as 5,000 interactions across the average life of a T cell (\sim 3 days) equates to approximately 1 antigen-presenting cell (APC)–T cell interaction per minute. We created a new biorepository of 4,500 granulomas, using this EE threshold for exhaustion. Using the same three granulomas as those in Fig. 4, we performed a spatial and temporal analysis (out to 200 days) to investigate the location of exhausted T cells within granulomas (Fig. 5). Figure 5A to C display the spatial location and magnitude of EE throughout the sterile (Fig. 5A), median CFU (Fig. 5B), and TB pneumonia (Fig. 5C) simulations, where dark blue represents high-density EE areas and white represents areas within the simulation that lack EE. Figure 5D to F reveal the spatial location of T cells as they exceed the EE threshold and become labeled with an exhaustion phenotype. Each simulation (sterile [Fig. 5D], median CFU [Fig. 5E], TB

pneumonia [Fig. 5F]) has its own scale ranging from white to dark blue; thus, comparison of one EE map to another simulation's EE map should not be performed. Figure 5G to I display a plot of the level of overall exhaustion, across time, as a cumulative percentage of all T cells that were activated in the granuloma simulation. As these simulations show, many granulomas show little cumulative exhaustion throughout the simulation. Note that the spatial locations of exhaustion are similar for each type of granuloma; T cells become exhausted only when they enter the center of the granuloma and can accrue sufficient EE. Further, the cumulative exhaustion plots reveal that across time, exhaustion accumulates faster at early time points (between days 25 and 50) than at later time points (between days 100 and 200). However, as the granuloma matures and organizes, T cell exposure events decline, and the rate of exhaustion lowers or stabilizes.

Based on the location of exhausted T cells in the simulations, it appears that cells are more likely to become exhausted as they penetrate deeper into the granuloma. As previously shown, *M. tuberculosis* bacilli are primarily located in the inner core of macrophages and within the necrotic center (51). As the structure becomes more organized, fewer T cells appear in this region. Thus, GranSim predicts that identifying large quantities of a T cell exhaustion phenotype is unlikely after granuloma formation.

Using our biorepository of nearly 3,000 simulated granulomas that matched all 44 NHP granulomas, we compared the observed levels of exhaustion (NHP granulomas) with those obtained from simulations (Fig. 6A). It is important to note that we did not calibrate to the exhaustion levels found in NHP data but instead calibrated the model to the NHP CFU and CD3⁺ T cell counts and then compared exhaustion levels within these simulations to those obtained from NHP studies. The average difference between pairs in these two populations was not significant. That is, overall, our model was able to recapitulate the observed levels of exhaustion.

Computational modeling allows us to artificially inflate the levels of T cell exhaustion in granulomas in order to test the impact of widespread T cell exhaustion on granuloma outcome. We selected the median bacterial burden simulation (Fig. 5B) and resimulated that same granuloma under a hypothetical condition of decreasing EE threshold. We reasoned that a lower EE threshold would result in a larger number of T cells becoming exhausted and a decreased ability of the granuloma to contain bacterial growth. We observe that inflated levels of exhaustion in the simulation lead to unfeasible granuloma outcomes, particularly in those granulomas whose EE threshold was less than 200 (Fig. 6B). The previous simulation with an EE threshold of 5,236 has a bacterial burden of about 288 CFU by day 200 (Fig. 6C), and the simulation with an EE of 1 has 115,192,400 CFU (Fig. 6D). To our knowledge and in our experience with macaque granulomas (52), these bacterial burdens are biologically unreasonable and can be attained computationally only when exhaustion levels are extremely high, well beyond the NHP findings. We conclude that T cell exhaustion alone cannot explain the low frequency of *M. tuberculosis*-responsive T cells in the granuloma, as the vast majority of T cells do not encounter stimulation by antigen sufficiently frequently to become exhausted.

DISCUSSION

The presence and effect of T cell exhaustion have been studied in many chronic diseases. The chronic nature of *M. tuberculosis* infection and continued presence of bacterial antigens in granulomas seemed to be an obvious scenario for the development of exhausted T cells, which could explain the inability of some granulomas to completely eliminate the organisms. However, in NHP models of TB, for both rhesus and cynomolgus macaques, we detected only limited apparent exhaustion of T cells within granulomas, based on the expression of inhibitory receptors. In fact, the small number of granuloma T cells expressing inhibitory receptors was apparently still functional and producing cytokines or proliferating at frequencies similar to those of T cells not expressing inhibitory receptors. We observed a modest negative correlation between the intensity of PD-1 expression (MFI) and T cell cytokine expression, sug-

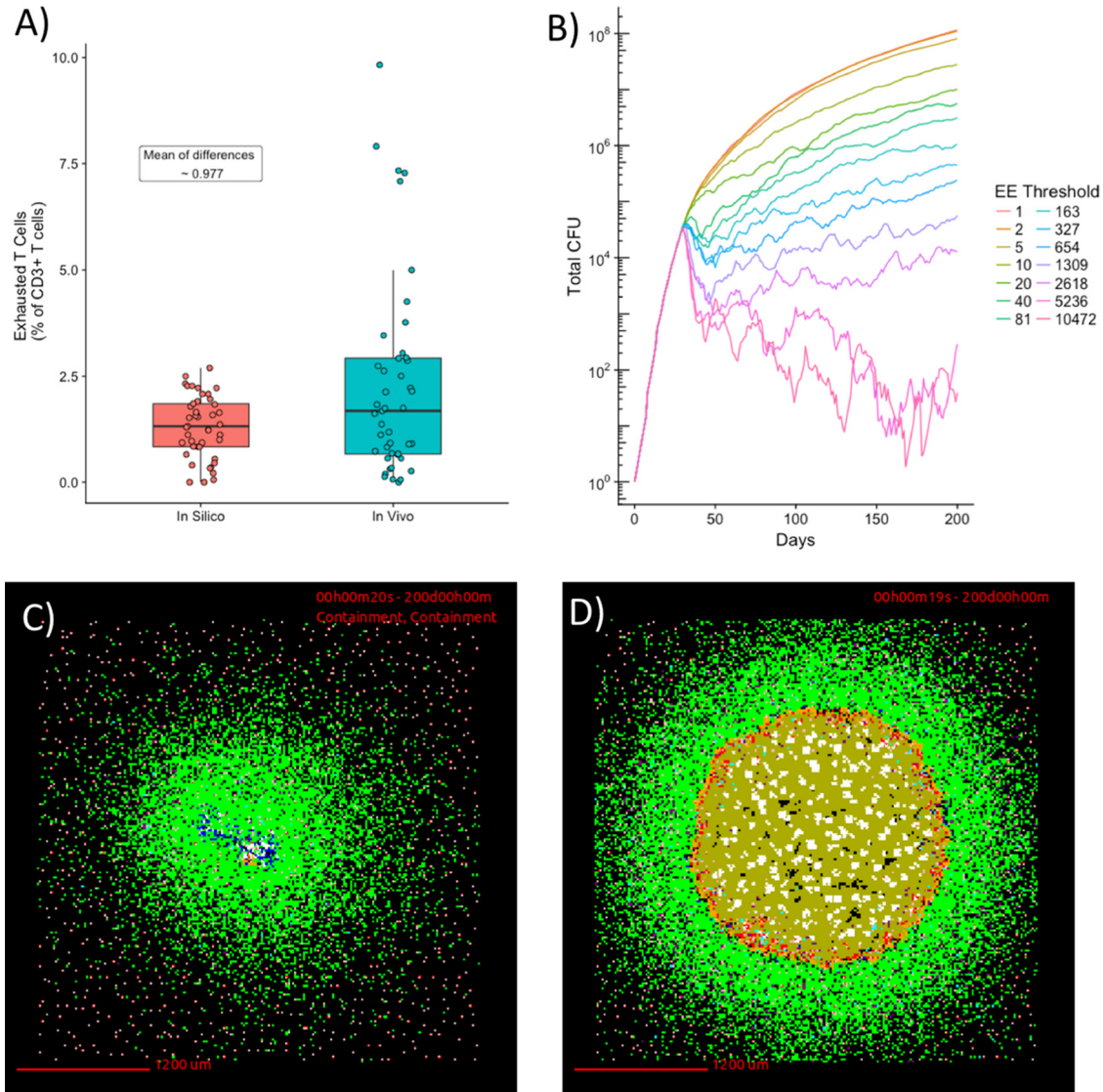


FIG 6 Artificially increasing T cell exhaustion levels result in bacterial burdens that are not observed experimentally. (A) A box-and-whisker plot demonstrating the distribution of exhaustion levels from NHP studies versus those obtained via simulation in the 44 macaque granulomas (blue) and the simulations that matched (red). (B) Graph of number of CFU versus time at various EE thresholds. (C) Snapshot of granuloma with an EE threshold of 5,236 taken at day 200. This granuloma represents a biologically feasible outcome and had a bacterial burden of 288 CFU. (D) Snapshot of granuloma with an EE threshold of 1 taken at day 200. This granuloma had a bacterial burden of 115,192,400 CFU.

gesting that T cells that express more PD-1 may be more likely to be exhausted, but there are few T cells strongly expressing PD-1 in TB granulomas. To further investigate the lack of apparent exhaustion in granulomas, we turned to our computational (agent-based) model of a granuloma, GranSim. We demonstrated that GranSim can match macaque granuloma data and then explored the extent of exhaustion in the simulated granulomas. Again, we found low levels of exhausted T cells in most granulomas. GranSim revealed that T cells could not readily penetrate into the macrophage or caseous layers of the granulomas, where most bacilli exist. Thus, the organized structure of the granuloma precludes widespread T cell exhaustion, in that macrophages and *M. tuberculosis* bacilli tend to be in the center of the granuloma, while T cells are concentrated in the lymphocyte cuff on the periphery of the granuloma. In fact, in cases of less-organized pathology (TB pneumonia), we did observe, experimentally and computationally, somewhat higher levels of exhaustion, although they were still relatively low. Finally, we used our computational model to artificially

inflate the level of T cell exhaustion in granulomas (by decreasing the threshold of T cell-APC interactions) and found that this would lead to exceptionally high bacterial burdens in granulomas. Such high bacterial burdens in individual granulomas are rarely seen in macaque models, even including those with substantial levels of disease. Thus, we conclude that limited T cell exhaustion in granulomas is due to the relative infrequency of T cells contacting *M. tuberculosis*-infected macrophages (or APCs carrying *M. tuberculosis* antigens), which is a key feature of the organized structure of granulomas.

Only low frequencies of T cells in TB granulomas expressed inhibitory receptors, despite being at the local site of *M. tuberculosis* persistence. Even the most frequently expressed inhibitory receptor in TB granulomas, PD-1, occurred much less frequently (~10% of CD8 T cells expressed PD-1) than T cells expressing PD-1 at the site of infection in other chronic infectious diseases (~55% of CD8 T cells in the liver of a hepatitis C virus-infected individual; ~40 to 50% of CD8 T cells in a rectal biopsy specimen of a simian immunodeficiency virus [SIV]-infected individual) (53, 54). With chronic *Brucella melitensis* infection, high frequencies of PD-1⁺ LAG-3⁺ CD8 T cells were also observed at the local site of infection, the spleen, compared to the extremely low levels in our TB granulomas (0.12% of CD8 T cells expressing PD-1⁺ LAG-3⁺) (55). Furthermore, like other inhibitory receptors, PD-1 is both an activation and an exhaustion marker. There was very little coexpression of multiple inhibitory receptors, with more coexpression of PD-1 with CD69, further suggesting that PD-1-expressing T cells in the granulomas are activated, not exhausted. Thus, we conjecture that the low levels of "inhibitory" receptor expression on granuloma-derived T cells actually represent activation markers. This alternative role of inhibitory receptors as markers for proliferating activated cells has been previously explored in *M. tuberculosis* infection and SIV infection. A study of PD-1⁺ T cells in mice during *M. tuberculosis* infection showed that these cells proliferated and were actually necessary for maintaining effector cells (27). Hong et al. also found a similar role for PD-1⁺ T cells during chronic SIV infections (34). The necessity of PD-1⁺ T cells for protection during *M. tuberculosis* infection was further highlighted by studies in PD-1 knockout mice that had high bacterial burdens and extreme inflammation (29, 30) in comparison to wild-type infected mice.

Although some of our data contradict other studies of T cell exhaustion in TB, we also observed some similar findings. Like the mouse model of TB, PD-1 was one of the most frequently expressed inhibitory markers on T cells (26). Unfortunately, we were unable to confirm the presence of TIM-3 on granuloma T cells because of the lack of a reliable antibody for NHPs. Although Phillips et al. showed higher LAG-3 expression on T cells from the lungs of *M. tuberculosis*-infected rhesus macaques, we saw much lower levels in individual granulomas from *M. tuberculosis*-infected cynomolgus and rhesus macaques, closer to the levels they observed in clinically latent animals (24). However, similar to Phillips et al., we observed high frequencies of LAG-3⁺ cells that were also not CD3⁺. Some of these discrepancies could be due to differences in the animal models used to investigate exhaustion in *M. tuberculosis* granulomas. *M. tuberculosis* infections in mice do not create the same structured organization in granulomas as observed in humans and NHPs, and therefore T cells may have more interactions with the *M. tuberculosis* bacilli, creating more opportunities for exhausted T cells. We used samples primarily, although not exclusively, from cynomolgus macaques in this study, which tend to have less severe disease than rhesus macaques, and thus we may have observed slightly lower expression of LAG-3 in lung granulomas than that of published studies on lung tissue from *M. tuberculosis*-infected rhesus macaques. There were also differences in timing. In the current study, we examined longer, more chronic infections than was done in previous mouse or rhesus studies, although our samples from early infections also had few T cells expressing inhibitory receptors. Most of the data from *M. tuberculosis*-infected patients is from peripheral blood, so we were unable to confirm our T cell exhaustion observations at the lung granuloma level to peripheral human data; however, we have previously shown that peripheral immune responses do not reflect local (granuloma) immune responses (6).

Our data support the likelihood that the lack of T cell exhaustion in a chronic disease like TB is a result of the unique characteristic of the disease—containment of the *M. tuberculosis* bacilli within a well-structured granuloma. While the close proximity of bacterial antigens to the host immune cells seemed to be an obvious environment for T cell exhaustion, the structure and spatial arrangement of the immune cells in the granuloma may be responsible for the low levels of T cell exhaustion. T cells infiltrate the granulomas early in infection, but during chronic infection (>3 months), the vast majority of T cells are on the outer periphery of the granuloma, away from the bacteria and exposed macrophages in the center of the granuloma, thus preventing low levels of *M. tuberculosis*-T cell interactions, as also previously suggested by Kauffman et al. (25). Likewise, we and Phillips et al. observed that T cells that express the inhibitory receptors tend to be on the outer edges of the granuloma (Fig. 2) (24).

An alternative hypothesis to T cell exhaustion that could explain the low levels of cytokine production by T cells in the granuloma is that many granuloma T cells are not specific for *M. tuberculosis* antigens. Unfortunately, tetramers for cynomolgus macaques currently do not exist, and the rhesus macaques used here were not major histocompatibility complex (MHC) typed; thus, the tetramers available could not be used. Therefore, we were unable to quantify the number of T cells specific for a single *M. tuberculosis* antigen in the granulomas and determine the frequency of T cell exhaustion within *M. tuberculosis*-specific T cells in the current study. As more reagents are developed, this is another strategy to pursue. In addition, the production of immunomodulatory cytokines, such as IL-10 or transforming growth factor β (TGF- β), or inflammation or oxygen or nitric oxide species in granulomas may regulate T cell function. The low frequency of cytokine-producing T cells may be a beneficial characteristic of lung granulomas. Sakai et al. suggested that in a mouse model of *M. tuberculosis* infection, increasing the IFN- γ production by CD4 T cells in lung tissue by reducing PD-1 inhibition exacerbated the bacterial burden within the lungs, worsening TB disease and shortening the host life span (28). Our data from macaque granulomas and our computational modeling indicate that a balance of anti-inflammatory (e.g., IL-10) and proinflammatory cytokines (TNF, IL-2) within a granuloma is correlated with lower bacterial burdens or sterilization (6, 47, 49). Studies to examine the T cell cytokine response relative to antigen specificity are under way.

Together, these data support and extend the notion that a balance of cytokine responses and T cell functionality are necessary for control of *M. tuberculosis* within granulomas and that due to the spatial organization of the granuloma, T cell exhaustion is likely not a major contributor to this balance at the local granuloma level.

MATERIALS AND METHODS

Experimental animals. Samples from 11 cynomolgus macaques (*Macaca fascicularis*) between 6.4 and 9.2 years of age, with starting weights of 5 to 7.8 kg (Valley Biosystems, Sacramento, CA), and four rhesus macaques (*Macaca mulatta*) between 5.1 and 14.8 years of age, with starting weights of 5.4 to 7.9 kg (Vaccine Research Center, NIH) were assessed in this study. Animal care was in accordance with institutional guidelines, and all experimental manipulations, protocols, and care of the animals were approved by the University of Pittsburgh School of Medicine Institutional Animal Care and Use Committee (IACUC). The animals were examined while in quarantine as previously described to ensure that they were in good physical health with no previous *M. tuberculosis* infection (56, 57). Samples were obtained for this study from NHPs from other studies and infected with 3 to 31 CFU of the virulent Erdman strain of *M. tuberculosis* by bronchoscopic instillation to the lower lung lobe, as previously described (58). In this study, 34 lung granulomas, 8 lung samples of complex TB disease (clusters, consolidations, pneumonia), and 15 *M. tuberculosis*-infected lymph nodes were analyzed.

Necropsy procedures, bacterial burden, and staining for flow cytometry. Necropsy was performed as previously described (56, 57). In summary, NHPs were humanely sacrificed by terminal bleed, and granulomas in lungs identified by positron emission tomography-computed tomography (PET-CT) or at necropsy were individually excised, with half of the granuloma homogenized into a single-cell suspension for bacterial burden and immunological assays and the other half used for histological analysis, size permitting. To determine the bacterial burden, each granuloma homogenate was plated in serial dilutions on 7H11 medium and incubated at 37°C in 5% CO₂ for 21 days before CFU enumeration.

Excised and homogenized granulomas were analyzed for immunological response by surface and intracellular staining and flow cytometry. For each granuloma, cells were resuspended in 1 ml of RPMI 1640 containing 1% HEPES, 1% L-glutamine, 10% human AB serum, and 0.1% brefeldin A (Golgiplug; BD Biosciences) and incubated for 2 to 3 h at 37°C in 5% CO₂ after homogenization to capture the cytokine

response. Our previous data indicate that additional *ex vivo* stimulation with *M. tuberculosis* antigens does not increase cytokine production and can lead to decreased cell recovery. In excised granulomas, *M. tuberculosis* and *M. tuberculosis* antigens are present and likely are restimulating T cells in the homogenized samples. After incubation, granuloma cells were washed with 1× phosphate-buffered saline (PBS) and stained for viability (Invitrogen). Granuloma cells were stained for surface markers, inhibitory receptors, and cytokines in the presence of 1% fetal bovine serum (FBS) in PBS. Antibodies for cell surface markers included the following: CD3 (clone SP34-2; BD Biosciences), CD4 (clone L200; BD Biosciences), CD8 (clone RPA-T8; BD Biosciences), and PD-1 (clone EH12.1; BD Biosciences). Cells were fixed and permeabilized (BD Biosciences). Intracellular staining of the following inhibitory receptors, activation and proliferation markers, and cytokines was done: LAG-3 (clone FAB23193P; R&D Biosystems), CTLA-4 (clone BNI3; BD Biosciences), CD69 (clone TP1.55.3; Beckman Coulter), Ki67 (clone B56; BD Biosciences), IFN- γ (clone B27; BD Biosciences), IL-2 (clone MQ1-17H12; BD Biosciences), and TNF (clone MAB11; BD Biosciences). Cells were fixed in 1% paraformaldehyde. Data acquisition was performed using an LSR II flow cytometer (BD Biosciences) and analyzed using FlowJo Software v.9.7 (Treestar, Inc.). The gating strategy is outlined in Fig. S1 in the supplemental material.

For the PD-1 and PD-L1 neutralization assay, a subset of lung granulomas and TB pneumonia samples from two cynomolgus macaques were excised and homogenized as described above. PBMCs were also isolated at the time of necropsy, as previously described (56). Single-cell suspensions were divided, and each half of the sample was incubated *ex vivo* with either (i) 10 μ g/ml goat polyclonal anti-human-PD-1 antibody (R&D Biosystems) and 10 μ g/ml goat polyclonal anti-human-PD-L1 antibody (R&D Biosystems) or (ii) with polyclonal goat IgG isotype (R&D Biosystems) in 150 μ l of RPMI 1640 containing 1% HEPES, 1% L-glutamine, and 10% human AB serum for 1.5 to 2.5 h at 37°C in 5% CO₂. After the initial incubation, additional *M. tuberculosis* peptide pools (ESAT-6 and CFP-10, 2 μ g/ml) were added to the samples to stimulate an *M. tuberculosis*-specific cytokine response in the presence of brefeldin A (Golgiplug; BD Biosystems) and incubated at 37°C in 5% CO₂ for an additional 2.5 h. Samples were then stained for viability, surface markers, inhibitory receptors, and cytokines and then collected and analyzed as described above.

Immunofluorescence of paraffin-embedded samples. Portions of granulomas excised during necropsy were formalin fixed, paraffin embedded, and consecutively cut in 5- μ m sections for histological analysis. For immunofluorescent assays, slides with two consecutive tissue sections were deparaffinized by xylene, followed by washes in 95% and 70% ethanol before antigen retrieval in Tris-EDTA (pH 9) under heat and pressure. Slides were cooled, washed with PBS, and blocked using 1% bovine serum albumin (BSA) in PBS, before incubation overnight at 4°C or 1 h at room temperature with primary antibodies against CD3 (clone CD3-12, Abcam; Dako), PD-1 (clone NAT105, Abcam), and LAG-3 (clone EPR4392, Abcam). Antibodies were tested in lymph node samples (Fig. S2). After washing with PBS, slides were stained with secondary anti-mouse, anti-rat, and anti-rabbit antibodies (Jackson Laboratories and Invitrogen) for 1 h at room temperature and coverslips were mounted with ProLong Gold with DAPI (Invitrogen). Confocal microscopy was performed using an Olympus microscope equipped with three lasers. Images were collected using a 20× objective at a size of 1,024 by 1,024 and then compiled using Adobe Photoshop before quantification. Individual cell numbers were identified using the open source image analysis software CellProfiler. To analyze larger granulomas, small regions of interest were selected and CellProfiler settings were modulated based on image quality so that relevant cell types were accurately quantified. Once pipelines were determined per image, both the isotype (secondary only staining) and the stained image were analyzed using the same parameters. Isotype image numbers were subtracted from stained images, resulting in an adjusted number representing the cells identified per tissue section.

Computational modeling with GranSim. All simulations utilize a two-dimensional (2D) hybrid, agent-based model (ABM) called GranSim that captures environmental, cellular, and bacterial dynamics across molecular, cellular, and tissue-scale events (44, 46, 59, 60). As an established model, GranSim has been calibrated extensively to data from a nonhuman primate model of TB (44–46, 59–64). At the molecular scale, GranSim incorporates cytokine and chemokine diffusion, secretion, and degradation. GranSim also tracks individual immune cells on a 2D simulation grid of microcompartments, including four macrophage states (resting, activated, infected, and chronically infected) and T cell types (cytotoxic, IFN- γ producing, and regulatory). Granuloma formation at the tissue level is an emergent behavior of GranSim. See <http://malthus.micro.med.umich.edu/GranSim> for full model details and an executable file. The following methods provide details on mechanisms added to GranSim so that we can use GranSim as a tool to study exhaustion in granulomas.

Model definitions, assumptions, and justifications. A great advantage of our *in silico* representation is that we can track cellular movement, behavior, and interaction across time. In GranSim, we define an interaction between a T cell and a macrophage by the occurrence of a macrophage entering the double Moore neighborhood of a T cell (65–67) (i.e., Moore neighborhood is defined as all microcompartments on the grid immediately adjacent to the one the cell is in; double Moore includes the next outer ring of microcompartments). In particular, as we evaluate the possibility of T cell exhaustion influencing the pathology of granuloma formation, we become solely interested in exposure events (EE), defined as the interactions between a T cell and an antigen-“exposed” macrophage.

In previous model versions, we defined an exposed macrophage according to three criteria: (i) if the cell contained any intracellular *M. tuberculosis*; (ii) if, within the single Moore neighborhood of the macrophage, there exists any live or dead extracellular *M. tuberculosis*, and (iii) if, within the single Moore neighborhood of the macrophage, there is another macrophage that was determined to be exposed

TABLE 2 Example analysis of *in silico* versus *in vivo* T cell exhaustion data^a

NHP Sample	Total CFU	CD3 Count	Matched Simulations
13516_RLL 17_20_cluster	2420	13810	5

Simulation Number (replication)	Mean Percent of Exhausted Cells
33(1)	0.0
33(2)	0.0
342(3)	0.0
877(1)	0.0
305(3)	3.3

Median Percent of Exhausted Cells in Matched Simulations	Percent of Exhausted Cells in NHP Samples
0.0	0.667

^aTable 2.3 displays the direct comparison between exhaustion in our matching simulations and the level of observed exhaustion in NHP samples. Tables 2.1 and 2.2 explain our method of matching and aggregating data. Table 2.1 displays 1 of the 44 NHP granuloma samples that we used for calibration. The right-most column shows the number of simulations that matched the NHP sample CFU values and CD3 count. Each simulation could match the criteria across several time points. Table 2.2 shows each of the five simulations that calibrated to NHP sample 13516_RLL 17_20 cluster and the average percentage of exhausted T cells across the simulation time points that matched NHP sample criteria. Finally, we aggregated the data to display an overall sense of model fit by selecting the “median of the means” for each matching simulation. Thus, for NHP sample 13516_RLL 17_20 cluster, the median percentage of exhaustion across all samples that matched was 0.0%. Flow cytometry data shows that this sample had 0.66% of T cells that showed two or more exhaustion markers.

during a previous time step. Additionally, once a macrophage becomes exposed, it remains exposed for the entirety of its life span (47).

As noted in the introduction, chronic antigenic stimulation is sufficient to develop exhaustion within a T cell population. Based on current literature, we model antigenic stimulation via EE (68–70). We use EE as a standard of stimulation across the lifetime of a T cell to evaluate various analytical measures about T cell exhaustion, including individual T cell exposure to antigens, average EE across T cell populations, and determination of whether only a few T cells out of the entire population accrue the majority burden of EE.

Finally, we created a new parameter within GranSim to introduce an exhausted T cell phenotype (this parameter was aptly named “exhaustion threshold”). If the EE of an IFN- γ -producing T cell or a cytotoxic T cell exceeds this preset threshold, then a T cell is marked as exhausted. Once labeled, it loses all effector function but continues to move around the grid until it dies from its natural life span (we do not assume there is an enhanced death rate for exhausted cells). Because we explore the possible role of exhaustion within granuloma formation, we crafted this parameter to represent the worst-case scenario: if a T cell exceeds the threshold, it immediately ceases effector function rather than, for example, exhibiting a progressive loss of function. Other formulations are possible, but we have considered this case as an upper bound for quantifying exhaustion levels (yielding the worst-case scenario).

Computational platform and post-run analysis. GranSim is constructed through use of the C++ programming language, Boost libraries (distributed under the Boost software license; <https://www.boost.org>), and the Qt framework for visualization (distributed under General Public License). The ABM is cross-platform (Macintosh, Windows, Unix) and runs with or without visualization software. GranSim model simulations were performed locally and also on the XSEDE’s OSG Condor pool resources.

We relied on uncertainty analysis (UA) techniques to explore model parameter space. In particular, we used Latin hypercube sampling (LHS) (reviewed in reference 50) for UA. The LHS algorithm is a stratified Monte Carlo sampling method without replacement (50) and was used to generate 1,500 unique parameter sets, which were simulated in replication three times (a total of 4,500 *in silico* simulations) for 200 days. When we matched our simulations to NHP granulomas, the sizes of the high and median bacterial burden samples often necessitated the use of a 200-by-200 microcompartment simulation space, whereas the simulation space for sterile samples could be performed within 100-by-100 microcompartments.

Analysis of statistical data derived on EE from simulations was performed using smoothScatter, ggplot2, and base packages in R (71) and Matlab (72). Additional analysis was conducted on more general data concerning granuloma-scale infection outcomes, granuloma formation, and concentration values of various effector molecules and CFU within the simulations.

Model calibration and definition of exhaustion. Once the model was updated, we recalibrated GranSim with respect to (i) CFU totals, (ii) CD3 totals, and (iii) time based on 44 separate NHP granuloma sample data. Table S2 in the supplemental material shows the parameter ranges we used to generate an *in silico* biorepository of 4,500 granulomas. Table 2 outlines a portion of the comprehensive analysis we performed to compare T cell exhaustion *in silico* with the data derived on T cell exhaustion *in vivo*.

Since the exact roles of individual inhibitory receptors as markers in the progression of T cell exhaustion is unclear (33), we assume that a T cell is only truly exhausted if it coexpresses any two or more inhibitory receptors. Thus, when we compared T cell exhaustion levels and markers *in vivo* against T cell exhaustion *in silico*, the *in vivo* percentage of T cells that are “exhausted” are actually the percentage of T cells that expressed two or more inhibitory receptors.

Of the 4,500 granulomas in our *in silico* biorepository, we matched simulations to samples according to our criteria, as shown in Table 2.1 of Table 2. As an example, if we examine NHP sample 13516_RLL 17_20, we were able to select five unique simulations that matched CFU and CD3 values across various simulation time points. For each of the five simulations, across every time point that matched the NHP sample’s CFU and CD3⁺ T cell levels, we found the average percentage of exhausted T cells (Table 2.2).

For example, the first replication of simulation 33 matched CFU and CD3 counts across five different time points over the 200-day simulation. We averaged the exhausted T cells across each of the 5 days and found that the mean percentage of exhausted T cells when this simulation matched our criteria was 0.0%.

Finally, we aggregated the data to provide a sense of overall model fit for each of the 44 NHP samples. Table 2.3 displays the median value across all the mean percentages of exhausted T cells for each sample's matching simulations. Thus, for sample 13516_RLL_17_20, the median percentage of exhaustion across all the samples that matched was 0.0%. Flow cytometry data show that this sample had 0.66% of T cells that displayed two or more inhibitory markers.

EE threshold selection. Initially, we created a biorepository of 4,500 granulomas using the LHS technique. Within this biorepository, the EE threshold for T cell exhaustion ranged from 200 to 10,000. The upper bound of the EE threshold of 10,000 interactions was selected because an exposed macrophage occupying every location in a T cell double Moore neighborhood for the lifetime of the T cell (average of 3 days in our simulation) would accrue 10,500 interactions. We selected 200 interactions as the lower level of EE because a T cell with 200 interactions has encountered exposed macrophages less than 2% of the time it has been alive—certainly a sufficient EE threshold for a phenotype that is caused by chronic stimulation.

Figures 5 and 6 were produced from a second biorepository of 4,500 granulomas. This biorepository was created with the exact same parameter ranges as those in Table S2 in the supplemental material, but the EE threshold was set to 5,236, the median of all simulations that matched the macaque granulomas. A threshold of 5,236 EE seems reasonable, as 4,320 interactions equals 1 interaction per minute through the average life span of a T cell.

Statistical analyses. Statistical analyses were conducted in GraphPad Prism 7 (GraphPad Software, San Diego, CA). Data were tested for normality by the D'Agostino-Pearson omnibus normality test. Since data analyzed in this study were not normally distributed but were paired, Wilcoxon matched-pair signed rank tests were used to compare two groups for multiple comparisons, with no multiple comparison adjustments to *P* values. Correlations were calculated by nonparametric Spearman rho tests. *P* values of ≤ 0.05 were considered significant and are noted in individual graphs or tables.

SUPPLEMENTAL MATERIAL

Supplemental material for this article may be found at <https://doi.org/10.1128/IAI.00426-18>.

SUPPLEMENTAL FILE 1, PDF file, 3.4 MB.

ACKNOWLEDGMENTS

We thank Paul Wolberg for computational programming assistance. We are grateful to Hannah Gideon, Joshua Mattila, Charles Scanga, and Pauline Maiello for technical assistance, as well as the veterinary technicians and all members of the Flynn laboratory for helpful discussions.

This research was supported by the following NIH grants awarded to J.L.F. and D.E.K.: R01 AI123093, U01HL131072, and R01 HL110811. This research also used resources of the National Energy Research Scientific Computing Center, which is supported by the Office of Science of the U.S. Department of Energy under contract no. DE-AC02-05CH11231, and by the Extreme Science and Engineering Discovery Environment (XSEDE), which is supported by National Science Foundation grant no. MCB140228.

The funders had no role in study design, data collection and interpretation, decision to publish, or preparation of the manuscript.

REFERENCES

1. WHO. January 2018. Tuberculosis fact sheet. <http://www.who.int/mediacentre/factsheets/fs104/en/>. Accessed 6 February 2018.
2. Ehlers S, Schaible UE. 2013. The granuloma in tuberculosis: dynamics of a host-pathogen collusion. *Front Immunol* 3:411. <https://doi.org/10.3389/fimmu.2012.00411>.
3. Lin PL, Flynn JL. 2010. Understanding latent tuberculosis: a moving target. *J Immunol* 185:15–22. <https://doi.org/10.4049/jimmunol.0903856>.
4. Russell DG. 2007. Who puts the tubercle in tuberculosis? *Nat Rev Microbiol* 5:39–47. <https://doi.org/10.1038/nrmicro1538>.
5. Flynn J, Chan J, Lin P. 2011. Macrophages and control of granulomatous inflammation in tuberculosis. *Mucosal Immunol* 4:271. <https://doi.org/10.1038/mi.2011.14>.
6. Gideon HP, Phuah J, Myers AJ, Bryson BD, Rodgers MA, Coleman MT, Maiello P, Rutledge T, Marino S, Fortune SM, Kirschner DE, Lin PL, Flynn JL. 2015. Variability in tuberculosis granuloma T cell responses exists, but a balance of pro- and anti-inflammatory cytokines is associated with sterilization. *PLoS Pathog* 11:e1004603. <https://doi.org/10.1371/journal.ppat.1004603>.
7. Zajac AJ, Blattman JN, Murali-Krishna K, Sourdive DJ, Suresh M, Altman JD, Ahmed R. 1998. Viral immune evasion due to persistence of activated T cells without effector function. *J Exp Med* 188:2205–2213. <https://doi.org/10.1084/jem.188.12.2205>.
8. Jiang Y, Li Y, Zhu B. 2015. T-cell exhaustion in the tumor microenvironment. *Cell Death Dis* 6:e1792. <https://doi.org/10.1038/cddis.2015.162>.
9. Boni C, Fiscaro P, Valdatta C, Amadei B, Di Vincenzo P, Giuberti T, Laccabue D, Zerbini A, Cavalli A, Missale G. 2007. Characterization of hepatitis B virus (HBV)-specific T-cell dysfunction in chronic HBV infection. *J Virol* 81:4215–4225. <https://doi.org/10.1128/JVI.02844-06>.
10. Urbani S, Amadei B, Tola D, Massari M, Schivazappa S, Missale G, Ferrari C. 2006. PD-1 expression in acute hepatitis C virus (HCV) infection is

- associated with HCV-specific CD8 exhaustion. *J Virol* 80:11398–11403. <https://doi.org/10.1128/JVI.01177-06>.
11. D'Souza M, Fontenot AP, Mack DG, Lozupone C, Dillon S, Meditz A, Wilson CC, Connick E, Palmer BE. 2007. Programmed death 1 expression on HIV-specific CD4⁺ T cells is driven by viral replication and associated with T cell dysfunction. *J Immunol* 179:1979–1987. <https://doi.org/10.4049/jimmunol.179.3.1979>.
 12. Day CL, Kaufmann DE, Kiepiela P, Brown JA, Moodley ES, Reddy S, Mackey EW, Miller JD, Leslie AJ, DePierres C. 2006. PD-1 expression on HIV-specific T cells is associated with T-cell exhaustion and disease progression. *Nature* 443:350. <https://doi.org/10.1038/nature05115>.
 13. Wherry EJ. 2011. T cell exhaustion. *Nat Immunol* 12:492–499. <https://doi.org/10.1038/ni.2035>.
 14. Buggert M, Frederiksen J, Lund O, Betts MR, Biague A, Nielsen M, Tauriainen J, Norrgren H, Medstrand P, Karlsson AC. 2016. CD4⁺ T cells with an activated and exhausted phenotype distinguish immunodeficiency during aviremic HIV-2 infection. *AIDS* 30:2415. <https://doi.org/10.1097/QAD.0000000000001223>.
 15. Pardoll DM. 2012. The blockade of immune checkpoints in cancer immunotherapy. *Nat Rev Cancer* 12:252–264. <https://doi.org/10.1038/nrc3239>.
 16. Ngoi SF, von Scheidt B, Akiba H, Yagita H, Teng MW, Smyth MJ. 2011. Anti-TIM3 antibody promotes T cell IFN- γ -mediated antitumor immunity and suppresses established tumors. *Cancer Res* 71:3540–3551. <https://doi.org/10.1158/0008-5472.CAN-11-0096>.
 17. Velu V, Titanji K, Zhu B, Husain S, Pladevega A, Lai L, Vanderford TH, Chennareddi L, Silvestri G, Freeman GJ. 2009. Enhancing SIV-specific immunity in vivo by PD-1 blockade. *Nature* 458:206–210. <https://doi.org/10.1038/nature07662>.
 18. Barber DL, Wherry EJ, Masopust D, Zhu B, Allison JP, Sharpe AH, Freeman GJ, Ahmed R. 2006. Restoring function in exhausted CD8 T cells during chronic viral infection. *Nature* 439:682–687. <https://doi.org/10.1038/nature04444>.
 19. Trautmann L, Janbazian L, Chomont N, Said EA, Gimmig S, Bessette B, Boulassel M-R, Delwart E, Sepulveda H, Balderas RS. 2006. Upregulation of PD-1 expression on HIV-specific CD8⁺ T cells leads to reversible immune dysfunction. *Nat Med* 12:1198. <https://doi.org/10.1038/nm1482>.
 20. Singh A, Mohan A, Dey AB, Mitra DK. 2013. Inhibiting PD-1 pathway rescues M. tuberculosis-specific IFN- γ producing T cells from apoptosis in tuberculosis patients. *J Infect Dis* 208:603–615. <https://doi.org/10.1093/infdis/jit206>.
 21. Shen L, Gao Y, Liu Y, Zhang B, Liu Q, Wu J, Fan L, Ou Q, Zhang W, Shao L. 2016. PD-1/PD-L pathway inhibits M.tb-specific CD4⁺ T-cell functions and phagocytosis of macrophages in active tuberculosis. *Sci Rep* 6:38362. <https://doi.org/10.1038/srep38362>.
 22. Jurado JO, Alvarez IB, Pasquinelli V, Martínez GJ, Quiroga MF, Abbate E, Musella RM, Chuluyan HE, García VE. 2008. Programmed death (PD)-1: PD-ligand 1/PD-ligand 2 pathway inhibits T cell effector functions during human tuberculosis. *J Immunol* 181:116–125. <https://doi.org/10.4049/jimmunol.181.1.116>.
 23. Day CL, Abrahams DA, Lerumo L, van Rensburg EJ, Stone L, O'rie T, Pienaar B, de Kock M, Kaplan G, Mahomed H. 2011. Functional capacity of Mycobacterium tuberculosis-specific T cell responses in humans is associated with mycobacterial load. *J Immunol* 187:2222–2232. <https://doi.org/10.4049/jimmunol.1101122>.
 24. Phillips BL, Mehra S, Ahsan MH, Selman M, Khader SA, Kaushal D. 2015. LAG3 expression in active Mycobacterium tuberculosis infections. *Am J Pathol* 185:820–833. <https://doi.org/10.1016/j.ajpath.2014.11.003>.
 25. Kauffman K, Sallin M, Sakai S, Kamenyeva O, Kabat J, Weiner D, Sutphin M, Schimel D, Via L, Barry C, III. 2018. Defective positioning in granulomas but not lung-homing limits CD4 T-cell interactions with Mycobacterium tuberculosis-infected macrophages in rhesus macaques. *Mucosal Immunol* 11:462–473. <https://doi.org/10.1038/mi.2017.60>.
 26. Jayaraman P, Jacques MK, Zhu C, Steblenko KM, Stowell BL, Madi A, Anderson AC, Kuchroo VK, Behar SM. 2016. TIM3 mediates T cell exhaustion during Mycobacterium tuberculosis infection. *PLoS Pathog* 12: e1005490. <https://doi.org/10.1371/journal.ppat.1005490>.
 27. Reiley WW, Shafiani S, Wittmer ST, Moon JJ, Jenkins MK, Urdahl KB, Winslow GM, Woodland DL. 2010. Distinct functions of antigen-specific CD4 T cells during murine Mycobacterium tuberculosis infection. *Proc Natl Acad Sci U S A* 107:19408–19413. <https://doi.org/10.1073/pnas.1006298107>.
 28. Sakai S, Kauffman KD, Sallin MA, Sharpe AH, Young HA, Ganusov VV, Barber DL. 2016. CD4 T cell-derived IFN- γ plays a minimal role in control of pulmonary Mycobacterium tuberculosis infection and must be actively repressed by PD-1 to prevent lethal disease. *PLoS Pathog* 12: e1005667. <https://doi.org/10.1371/journal.ppat.1005667>.
 29. Barber DL, Mayer-Barber KD, Feng CG, Sharpe AH, Sher A. 2011. CD4 T cells promote rather than control tuberculosis in the absence of PD-1-mediated inhibition. *J Immunol* 186:1598–1607. <https://doi.org/10.4049/jimmunol.1003304>.
 30. Lázár-Molnár E, Chen B, Sweeney KA, Wang EJ, Liu W, Lin J, Porcelli SA, Almo SC, Nathenson SG, Jacobs WR. 2010. Programmed death-1 (PD-1)-deficient mice are extraordinarily sensitive to tuberculosis. *Proc Natl Acad Sci U S A* 107:13402–13407. <https://doi.org/10.1073/pnas.1007394107>.
 31. Tousif S, Singh Y, Prasad DVR, Sharma P, Van Kaer L, Das G. 2011. T cells from Programmed Death-1 deficient mice respond poorly to Mycobacterium tuberculosis infection. *PLoS One* 6:e19864. <https://doi.org/10.1371/journal.pone.0019864>.
 32. Larbi A, Fulop T. 2014. From “truly naïve” to “exhausted senescent” T cells: when markers predict functionality. *Cytometry A* 85:25–35. <https://doi.org/10.1002/cyto.a.22351>.
 33. Yi JS, Cox MA, Zajac AJ. 2010. T-cell exhaustion: characteristics, causes and conversion. *Immunology* 129:474–481. <https://doi.org/10.1111/j.1365-2567.2010.03255.x>.
 34. Hong JJ, Amancha PK, Rogers K, Ansari AA, Villinger F. 2013. Re-evaluation of PD-1 expression by T cells as a marker for immune exhaustion during SIV infection. *PLoS One* 8:e60186. <https://doi.org/10.1371/journal.pone.0060186>.
 35. Hokey DA, Johnson FB, Smith J, Weber JL, Yan J, Hirao L, Boyer JD, Lewis MG, Makedonas G, Betts MR. 2008. Activation drives PD-1 expression during vaccine-specific proliferation and following lentiviral infection in macaques. *Eur J Immunol* 38:1435–1445. <https://doi.org/10.1002/eji.200737857>.
 36. Flynn JL, Klein E. 2011. Pulmonary tuberculosis in monkeys, p 83–105. *In* Leong FJ, Dartois V, Dick T (ed), A color atlas of comparative pathology of pulmonary tuberculosis. CRC Press, Boca Raton, FL.
 37. Crawford A, Angelosanto JM, Kao C, Doering TA, Odorizzi PM, Barnett BE, Wherry EJ. 2014. Molecular and transcriptional basis of CD4⁺ T cell dysfunction during chronic infection. *Immunity* 40:289–302. <https://doi.org/10.1016/j.immuni.2014.01.005>.
 38. Blackburn SD, Shin H, Haining WN, Zou T, Workman CJ, Polley A, Betts MR, Freeman GJ, Vignali DA, Wherry EJ. 2009. Coregulation of CD8⁺ T cell exhaustion by multiple inhibitory receptors during chronic viral infection. *Nat Immunol* 10:29–37. <https://doi.org/10.1038/ni.1679>.
 39. Triebel F, Jitsukawa S, Baixeras E, Roman-Roman S, Genevée C, Viegas-Pequignot E, Hercend T. 1990. LAG-3, a novel lymphocyte activation gene closely related to CD4. *J Exp Med* 171:1393–1405. <https://doi.org/10.1084/jem.171.5.1393>.
 40. Kisielow M, Kisielow J, Capoferri-Sollami G, Karjalainen K. 2005. Expression of lymphocyte activation gene 3 (LAG-3) on B cells is induced by T cells. *Eur J Immunol* 35:2081–2088. <https://doi.org/10.1002/eji.200526090>.
 41. Workman CJ, Wang Y, El Kasmi KC, Pardoll DM, Murray PJ, Drake CG, Vignali DA. 2009. LAG-3 regulates plasmacytoid dendritic cell homeostasis. *J Immunol* 182:1885–1891. <https://doi.org/10.4049/jimmunol.0800185>.
 42. Becker M, De Bastiani MA, Parisi MM, Guma FT, Markoski MM, Castro MA, Kaplan MH, Barbé-Tuana FM, Klamt F. 2015. Integrated transcriptomics establish macrophage polarization signatures and have potential applications for clinical health and disease. *Sci Rep* 5:13351. <https://doi.org/10.1038/srep13351>.
 43. Wherry EJ, Blattman JN, Murali-Krishna K, Van Der Most R, Ahmed R. 2003. Viral persistence alters CD8 T-cell immunodominance and tissue distribution and results in distinct stages of functional impairment. *J Virol* 77:4911–4927. <https://doi.org/10.1128/JVI.77.8.4911-4927.2003>.
 44. Segovia-Juarez JL, Ganguli S, Kirschner D. 2004. Identifying control mechanisms of granuloma formation during M. tuberculosis infection using an agent-based model. *J Theor Biol* 231:357–376. <https://doi.org/10.1016/j.jtbi.2004.06.031>.
 45. Ray JCJ, Flynn JL, Kirschner DE. 2009. Synergy between individual TNF-dependent functions determines granuloma performance for controlling Mycobacterium tuberculosis infection. *J Immunol* 182:3706–3717. <https://doi.org/10.4049/jimmunol.0802297>.
 46. Fallahi-Sichani M, El-Kebir M, Marino S, Kirschner DE, Linderman JJ. 2011. Multiscale computational modeling reveals a critical role for TNF- α

- receptor 1 dynamics in tuberculosis granuloma formation. *J Immunol* 186:3472–3483. <https://doi.org/10.4049/jimmunol.1003299>.
47. Cilfone NA, Ford CB, Marino S, Mattila JT, Gideon HP, Flynn JL, Kirschner DE, Linderman JJ. 2015. Computational modeling predicts IL-10 control of lesion sterilization by balancing early host immunity-mediated antimicrobial responses with caseation during Mycobacterium tuberculosis infection. *J Immunol* 194:664–677. <https://doi.org/10.4049/jimmunol.1400734>.
 48. Pienaar E, Cilfone NA, Lin PL, Dartois V, Mattila JT, Butler JR, Flynn JL, Kirschner DE, Linderman JJ. 2015. A computational tool integrating host immunity with antibiotic dynamics to study tuberculosis treatment. *J Theor Biol* 367:166–179. <https://doi.org/10.1016/j.jtbi.2014.11.021>.
 49. Warsinske HC, Pienaar E, Linderman JJ, Mattila JT, Kirschner DE. 2017. Deletion of TGF-beta1 increases bacterial clearance by cytotoxic T cells in a tuberculosis granuloma model. *Front Immunol* 8:1843. <https://doi.org/10.3389/fimmu.2017.01843>.
 50. Marino S, Hogue IB, Ray CJ, Kirschner DE. 2008. A methodology for performing global uncertainty and sensitivity analysis in systems biology. *J Theor Biol* 254:178–196. <https://doi.org/10.1016/j.jtbi.2008.04.011>.
 51. Mattila JT, Ojo OO, Kepka-Lenhart D, Marino S, Kim JH, Eum SY, Via LE, Barry CE, Klein E, Kirschner DE. 2013. Microenvironments in tuberculous granulomas are delineated by distinct populations of macrophage subsets and expression of nitric oxide synthase and arginase isoforms. *J Immunol* 191:773–784. <https://doi.org/10.4049/jimmunol.1300113>.
 52. Maiello P, DiFazio RM, Cadena AM, Rodgers MA, Lin PL, Scanga CA, Flynn JL. 2018. Rhesus macaques are more susceptible to progressive tuberculosis than cynomolgus macaques: a quantitative comparison. *Infect Immun* 86:e00505-17. <https://doi.org/10.1128/IAI.00505-17>.
 53. Radziejewicz H, Ibegbu CC, Fernandez ML, Workowski KA, Obideen K, Wehbi M, Hanson HL, Steinberg JP, Masopust D, Wherry EJ. 2007. Liver-infiltrating lymphocytes in chronic human hepatitis C virus infection display an exhausted phenotype with high levels of PD-1 and low levels of CD127 expression. *J Virol* 81:2545–2553. <https://doi.org/10.1128/JVI.02021-06>.
 54. Amancha PK, Hong JJ, Rogers K, Ansari AA, Villinger F. 2013. In vivo blockade of the programmed cell death-1 pathway using soluble recombinant PD-1-Fc enhances CD4⁺ and CD8⁺ T cell responses but has limited clinical benefit. *J Immunol* 191:6060–6070. <https://doi.org/10.4049/jimmunol.1302044>.
 55. Durward-Dioioia M, Harms M, Hall C, Smith JA, Splitter GA. 2015. CD8⁺ T cell exhaustion, suppressed gamma interferon production, and delayed memory response induced by chronic *Brucella melitensis* infection. *Infect Immun* 83:4759–4771. <https://doi.org/10.1128/IAI.01184-15>.
 56. Lin PL, Pawar S, Myers A, Pegu A, Fuhrman C, Reinhart TA, Capuano SV, Klein E, Flynn JL. 2006. Early events in Mycobacterium tuberculosis infection in cynomolgus macaques. *Infect Immun* 74:3790–3803. <https://doi.org/10.1128/IAI.00064-06>.
 57. Lin PL, Rodgers M, Smith L, Bigbee M, Myers A, Bigbee C, Chiosea I, Capuano SV, Fuhrman C, Klein E, Flynn JL. 2009. Quantitative comparison of active and latent tuberculosis in the cynomolgus macaque model. *Infect Immun* 77:4631–4642. <https://doi.org/10.1128/IAI.00592-09>.
 58. Capuano SV, Croix DA, Pawar S, Zinovic A, Myers A, Lin PL, Bissel S, Fuhrman C, Klein E, Flynn JL. 2003. Experimental Mycobacterium tuberculosis infection of cynomolgus macaques closely resembles the various manifestations of human M. tuberculosis infection. *Infect Immun* 71:5831–5844. <https://doi.org/10.1128/IAI.71.10.5831-5844.2003>.
 59. Ray JCJ, Wang J, Chan J, Kirschner DE. 2008. The timing of TNF and IFN- γ signaling affects macrophage activation strategies during Mycobacterium tuberculosis infection. *J Theor Biol* 252:24–38. <https://doi.org/10.1016/j.jtbi.2008.01.010>.
 60. Cilfone NA, Perry CR, Kirschner DE, Linderman JJ. 2013. Multi-scale modeling predicts a balance of tumor necrosis factor- α and interleukin-10 controls the granuloma environment during Mycobacterium tuberculosis infection. *PLoS One* 8:e68680. <https://doi.org/10.1371/journal.pone.0068680>.
 61. Fallahi-Sichani M, Kirschner DE, Linderman JJ. 2012. NF- κ B signaling dynamics play a key role in infection control in tuberculosis. *Front Physiol* 3:170. <https://doi.org/10.3389/fphys.2012.00170>.
 62. Fallahi-Sichani M, Schaller MA, Kirschner DE, Kunkel SL, Linderman JJ. 2010. Identification of key processes that control tumor necrosis factor availability in a tuberculosis granuloma. *PLoS Comput Biol* 6:e1000778. <https://doi.org/10.1371/journal.pcbi.1000778>.
 63. Fallahi-Sichani M, Flynn JL, Linderman JJ, Kirschner DE. 2012. Differential risk of tuberculosis reactivation among anti-TNF therapies is due to drug binding kinetics and permeability. *J Immunol* 188:3169–3178. <https://doi.org/10.4049/jimmunol.1103298>.
 64. Marino S, Sud D, Plessner H, Lin PL, Chan J, Flynn JL, Kirschner DE. 2007. Differences in reactivation of tuberculosis induced from anti-TNF treatments are based on bioavailability in granulomatous tissue. *PLoS Comput Biol* 3:1909–1924. <https://doi.org/10.1371/journal.pcbi.0030194>.
 65. Mirsky HP, Miller MJ, Linderman JJ, Kirschner DE. 2011. Systems biology approaches for understanding cellular mechanisms of immunity in lymph nodes during infection. *J Theor Biol* 287:160–170. <https://doi.org/10.1016/j.jtbi.2011.06.037>.
 66. Riggs T, Walts A, Perry N, Bickle L, Lynch JN, Myers A, Flynn J, Linderman JJ, Miller MJ, Kirschner DE. 2008. A comparison of random vs. chemotaxis-driven contacts of T cells with dendritic cells during repertoire scanning. *J Theor Biol* 250:732–751. <https://doi.org/10.1016/j.jtbi.2007.10.015>.
 67. Castellino F, Huang AY, Altan-Bonnet G, Stoll S, Scheinecker C, Germain RN. 2006. Chemokines enhance immunity by guiding naive CD8⁺ T cells to sites of CD4⁺ T cell-dendritic cell interaction. *Nature* 440:890. <https://doi.org/10.1038/nature04651>.
 68. Utzschneider DT, Alfei F, Roelli P, Barras D, Chennupati V, Darbre S, Delorenzi M, Pinschewer DD, Zehn D. 2016. High antigen levels induce an exhausted phenotype in a chronic infection without impairing T cell expansion and survival. *J Exp Med* 213:1819–1834. <https://doi.org/10.1084/jem.20150598>.
 69. Zuniga El, Harker JA. 2012. T-cell exhaustion due to persistent antigen: quantity not quality? *Eur J Immunol* 42:2285–2289. <https://doi.org/10.1002/eji.201242852>.
 70. Bucks CM, Norton JA, Boesteanu AC, Mueller YM, Katsikis PD. 2009. Chronic antigen stimulation alone is sufficient to drive CD8⁺ T cell exhaustion. *J Immunol* 182:6697–6708. <https://doi.org/10.4049/jimmunol.0800997>.
 71. The R Development Core Team. 2016. R: a language and environment for statistical computing. R Foundation for Statistical Computing, Vienna, Austria. <https://www.r-project.org/>.
 72. MathWorks, Inc. 2011. MATLAB. The MathWorks, Inc., Natick, MA.